Uncoupling Protein 3 Catalyzes the Exchange of C4 Metabolites Similar to UCP2

Jürgen Kreiter , Tatyana Tyschuk , Elena E Pohl *

Posted Date: 18 December 2023

doi: 10.20944/preprints202312.1214.v1

Keywords: SLC25 protein family; substrate transport; aspartate; malonate; malate; sulfate

Article

Uncoupling Protein 3 Catalyzes the Exchange of C4 Metabolites Similar to UCP2.

Jürgen Kreiter [1,2,†], Tatiana Tyshchuk [1,†] and Elena E. Pohl [1,*]

[1] Institute of Physiology, Pathophysiology and Biophysics, University of Veterinary Medicine, A-1210 Vienna, Austria
[2] Current address: Institute of Molecular and Cellular Physiology, Stanford Medical School, 94305 Stanford, CA, USA
[3] Current address: Ludwig Boltzmann Institute for Experimental and Clinical Traumatology in the AUVA Trauma Research Centre, 1200, Vienna, Austria
* Corresponding author. Email: elena.pohl@vetmeduni.ac.at
† Equally contributed.

Abstract: Uncoupling protein 3 (UCP3) belongs to the mitochondrial carrier protein superfamily SLC25 and is abundant in brown adipose tissue (BAT), heart and muscles. The expression of UCP3 in tissues mainly dependent on fatty acid oxidation suggests its involvement in cellular metabolism and has drawn attention to its possible transport function beyond the transport of protons in the presence of fatty acids. Based on the high homology between UCP2 and UCP3, we hypothesized that UCP3 transports C4 metabolites similar to UCP2. To test this, we measured the transport of substrates against phosphate ($^{32}P_i$) in proteoliposomes reconstituted with recombinant murine UCP3 (mUCP3). We found that mUCP3 mainly transports aspartate and sulfate but also malate, malonate, oxaloacetate and succinate. The transport rates calculated from the exchange of ^{32}Pi against extraliposomal aspartate and sulfate were 23.9 ± 5.8 and 17.5 ± 5.1 µmol/min/mg, respectively. Using site-directed mutagenesis we revealed that mutation of R84 resulted in impaired aspartate/phosphate exchange, demonstrating its critical role in substrate transport. Difference in substrate preference between mUCP2 and mUCP3 may be explained by their different tissue expression pattern and biological function in these tissues.

Keywords: SLC25 protein family; substrate transport; aspartate; malonate; malate; sulfate

Introduction

Mitochondrial uncoupling proteins (UCPs) are a subfamily of membrane protein homologues belonging to the solute carrier superfamily SLC25 [1–6]. UCP1 is the most prominent subfamily member abundant in brown adipose tissue (BAT), where it mediates non-shivering thermogenesis under cold-acclimated conditions [7–11]. UCP1 catalyses a fatty acid (FA)-dependent proton transport [12–16] across the inner mitochondrial membrane (IMM). It leads to the uncoupling of the transmembrane proton gradient, generated by oxidative phosphorylation, from ATP production and the generation of heat.

After being discovered in 1997 [17,18], UCP2 and UCP3 were identified as potential uncouplers due to their sequence homology with UCP1, their ability to decrease the mitochondrial membrane potential and increase membrane conductance for protons [19,20]. The latter was demonstrated in experiments on proteoliposomes [21,22] or lipid bilayer membranes [23,24] reconstituted with the recombinant UCP2 and UCP3. Their role in non-shivering thermogenesis has been discounted primarily due to the low protein amount in tissues [25]. Instead, it has been suggested that UCP2 and UCP3 could regulate proton leakage to reduce the formation of reactive oxygen species (ROS) [26,27].

The expression of UCP2 and UCP3 has been linked to a specific cell metabolism type [28,29]. UCP2 was found in cells and tissues that mainly rely on aerobic glycolysis, such as immune, stem and cancer cells [30–32]. These cell types were shown to predominantly convert glucose to lactate even in the presence of oxygen (Warburg effect). In addition to proton transport in the presence of

 doi:10.20944/preprints202312.1214.v1

FA [23], UCP2 catalyzes the exchange of various C4 metabolites for phosphate plus a proton as demonstrated in cell and artificial systems [33,34]. UCP3 is abundant in BAT, heart, and skeletal muscle [28,35–37], tissues that predominantly rely on FA oxidation. With emerging evidence for substrate transport catalyzed by other UCPs [38,39], the focus ought to fall on UCP3 as the closest homologue of UCP2. UCP3 shares 72% of sequence homology with human and 73% with mouse UCP2 [28]. The homology is particularly high in the putative substrate translocation pathway [40] (Figure 1A). It is especially striking when compared to another member of SLC25 superfamily with dual function, the adenine nucleotide translocase (ANT1, Figure 1B). In addition to its nucleotide transport function, a proton transporting function in the presence of long-chain fatty acids (FA) has been proposed for ANT1 [41–43]. According to the proposed transport mechanism FA anion, nucleotides (ATP, ADP) and substrate transport inhibitors (carboxyatractyloside and bongkrekic acid) compete for the same binding site R79 [44].

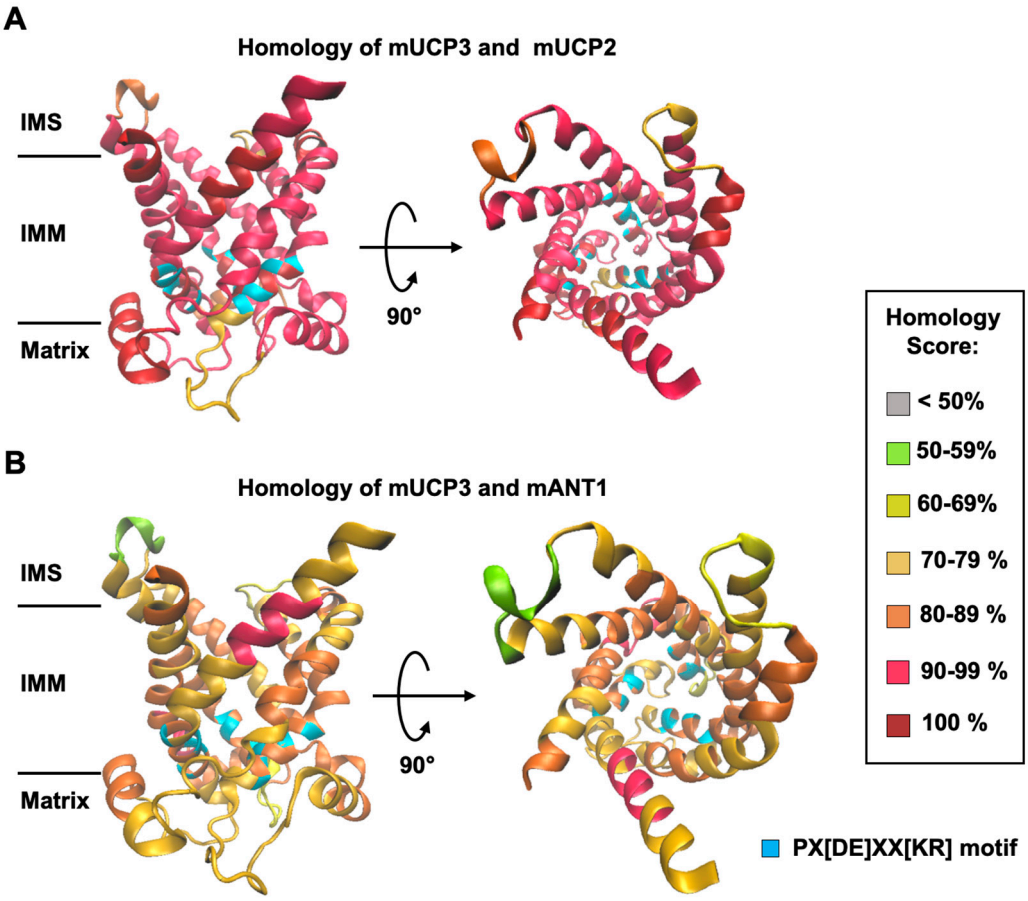

Figure 1. Homology of mUCP3 to mUCP2 and mANT1 mapped on a structural model of mUCP3. Cartoon representation of the structural model of UCP3 derived via mapping over the crystallographic structure of ANT1 (PDB code: 1OKC). Homology score between mUCP2 and mUCP3 (A) and mANT1 and mUCP3 (B) was assessed in 10 amino acid intervals. Structures are shown from the side (left) and top (right). Abbreviations are IMS - intermembrane space; IMM - inner mitochondrial membrane. The blue color denotes the mitochondrial carrier motif PX[DE]XX[KR], which is present in all mitochondrial carriers of the SLC25 family.

In the present study, we hypothesized that UCP3 may catalyze an efficient exchange of various C4 metabolites against radioactively labelled phosphate similar to UCP2, but with a difference in the substrate transport preferences resulting from their cell metabolism-dependent tissue expression. In addition, the critical binding site for the substrate and FA anion may be the same as recently shown for ANT1 [44]. To test these hypotheses, we reconstituted a purified recombinant mouse UCP3

 doi:10.20944/preprints202312.1214.v1

(mUCP3) and its mutant mUCP3-R79S into liposomes and measured the exchange rates of different C4 metabolites against radiolabeled phosphate.

Materials and methods

2.1. Chemicals

Unless otherwise mentioned, all chemicals were purchased in highest purity from Sigma Aldrich GmbH, Merck Millipore, or Carl Roth GmbH. Lipids 1,2-dioleoyl-sn-glycero-3-phosphocholine (DOPC), 1,2-dioleoyl-sn-glycero-3-phospho-ethanolamine (DOPE) and cardiolipin (CL) were from Avanti Polar Lipids Inc. (Alabaster, AL, USA). Radioactive substrates [2,5',8-^{3}H]-ATP, ^{14}C-L-malic acid and ^{32}P-phosphate were obtained from Perkin Elmer (Waltham, MA, USA).

2.2. Homology modelling of mouse UCP3 and homology score calculation.

Homology model of mUCP3 was made using the SWISS-MODEL Workspace/ GMQE [45]. The tertiary structure of protein was computed using the amino acid sequence of mUCP3 (Uniprot #: P56501) and the crystallographic structure of bovine ADP/ATP carrier (PDB:1OKC, [46]). Sequence homology scores between mUCP3 and mUCP2 (Uniprot #: P70406) and mANT1 (Uniprot #: P48962) were calculated in 10 amino acid increments from the sequence alignments (Figure S1), using the Sim Alignment Tool (https://web.expasy.org/sim/) and coloured as depicted in Figure 1.

2.3. Production and reconstitution of recombinant proteins into liposomes.

Expression, induction, inclusion body isolation and reconstitution into liposomes of mUCP3, mUCP2 and mANT1 were performed as described elsewhere [24,47,48]. In brief, the open reading frame of mUCP3, mUCP2 or ANT1 was added to the E. coli expression strain Rosetta. Inclusion bodies containing the target protein were extracted by cell disruption using a French press and resuspended into TE/G buffer (100 mM Tris at pH 7.5, 5 mM EDTA and 10% v/v glycerin) containing 2% w/v lauroylsarcosine. For protein reconstitution, 1 mg protein from inclusion bodies was solubilized in TE/G-buffer containing 2% SLS and 1 mM DTT and mixed gradually with 50 mg lipid mixture (DOPC:DOPE:CL - 45:45:10 mol%) dissolved in TE/G-buffer with the addition of 1.3% Triton X-114, 0.3% octylpolyoxyethylene, 1 mM DTT and 2 mM GTP. After overnight incubation, the mixture was concentrated using Amicon® Ultra-15 filters (Millipore, Schwalbach, Germany), dialyzed for 2 h against 1 L of TE/G- buffer containing 1 mg/ml BSA and 1 mM DTT and then dialyzed twice overnight against 1 L of TE/G without DTT. Buffer exchange was performed by three dialyses against 1 L of assay buffer (50 mM Na_2SO_4, 10 mM MES, 10 mM Tris, 0.6 mM EGTA at pH = 7.35). Aggregated and unfolded proteins were removed by centrifugation of the dialysate at 14,000×g and application of a 0.5 g hydroxyapatite column (Bio-Rad, Munich, Germany). GTP, initially added for the protein stabilization, was diluted 7-fold, so that the amount of GTP in the proteoliposomes was negligible.

Remaining detergent was removed by incubating twice with Bio-Beads SM-2 (Bio-Rad, Germany). The protein content of proteoliposomes was determined by Micro BCA Protein Assay (Perbio Science Deutschland GmbH, Bonn, Germany). The protein purity was verified by silver staining (Figure S2). Proteoliposomes were stored at − 80 °C until used, but not longer than two months.

2.4. Formation of unilamellar liposomes.

DOPE, DOPC and CL lipids were mixed in chloroform in 45:45:10 mol% concentration and evaporated under nitrogen flow until a fine film is formed on the wall of the glass vial. To ensure full evaporation of chloroform, the vial was connected to a vacuum pump for 30 min. Assay buffer (50 mM Na_2SO_4, 10 mM TRIS, 10 mM MES, 0.6 mM EGTA; pH = 7.34) was added to the lipids and the solution is vortexed to dissolve the lipids. Lipids were mixed with mUCP2 -, or mUCP3 - or ANT1 - containing liposomes to reach a final lipid concentration of 4 mg/ml and a protein to lipid ratio of 4

 doi:10.20944/preprints202312.1214.v1

µg/(mg of lipid). For empty liposomes, the lipid mixture was dissolved to 4 mg/ml with assay buffer. Liposomes were then incubated with 2 mM of phosphate (Pi) or malate and 10 to 50 µL ^{32}P-Pi or 10 µL ^{14}C-malate as tracer. Unilamellar liposomes were formed with an extruder (Avanti Polar Lipids, Inc., Alabaster, Alabama, US) using a 400 nm polycarbonate pore filter followed by membrane filter with a 100 nm pore diameter. Unincorporated substrates were removed via size exclusion chromatography. The homogeneity of the liposomal size was continuously verified by dynamic light scattering (Zetasizer, Malvern Panalytical Ltd, UK).

2.5. Radioactive transport assay

Release of intraliposomal substrates was initiated by adding 2 mM of the chosen non-radioactive substrate to the extraliposomal volume. Substrate exchange was stopped at t = 10 s, 60 s and 600 s by adding the sample to 30 ml size exclusion resin. Initial radioactivity of the (proteo-) liposomes was assessed by adding the sample to the resin before adding extraliposomal substrates. For each time point, the first 20 ml from the flow-through was collected in 4 x 5 ml fractions to (i) measure the peak signal, corresponding to the remaining amount of radioactive substrate in the (proteo-)liposomes and (ii) to collect the background signal as a quality control. Peak radioactivity was usually found in fraction 2 and 3, while the background signal was obtained in fraction 1 and 4. To each fraction, 10 mL of scintillation cocktail was added, and radioactivity measured by liquid scintillation counting (Tri-Carb 2100TR, Perkin Elmer). Inhibitors were added prior to liposome formation and were present intraliposomal and in the bulk solution to account for the random orientation of UCP3 in the membrane.

2.6. Determination of exchange rates

Data is represented by the remaining radioactive substrate, which is the counts per minute (CPM) of the radioactive substrates over time divided by the CPM from t = 0 s. The data was then fitted to an exponential function, where $\mathbf{y_0}$, **a** and **b** are the fitting parameters.

$$y(t) = y_0 + a \cdot e^{-b \cdot t} \quad (1)$$

$$y_0 + a = 1 \quad (2)$$

Equation (2) is required to meet the starting condition. The exchange rate $\boldsymbol{k}$ is then derived from the initial slope of the exponential function, where $[X_0]$ = 2 mM is the starting concentration of the respective radioactive substrate:

$$k = -[X_0]\frac{\partial}{\partial t}y(t) = [X_0] \cdot a \cdot b \quad (3)$$

2.7. Site-directed mutagenesis

In vitro site-directed mutagenesis was carried out on expression plasmids containing the cDNA of mUCP3 as templates. The mutation was introduced with designed oligonucleotides to alter mUCP3 Arg84 (CGC) to Gln (CAG) (R84Q) using a QuikChange II site-directed mutagenesis kit (Agilent, Austria). Successful mutations of the expression plasmids were confirmed by sequencing. Mutant mUCP3 expression plasmids were transformed in the E. coli expression strain Rosetta. Expression, induction, inclusion body isolation and reconstitution into liposomes of mUCP3 mutant were performed as described above.

2.8. Docking of phosphate and malate to UCP3

The structure of UCP3 was prepared for docking by removal of non-standard residues, non-complexed ions, addition of hydrogen, and assignment of Gasteiger charges in UCSF Chimera [49]. The ligand structures (phosphate and malate) were retrieved from the ZINC database (https://zinc.docking.org/, accessed last on 27 February 2023). Static docking was performed using

 doi:10.20944/preprints202312.1214.v1

AutoDock [50,51], embedded in UCSF Chimera. The grid box was set around putative binding site. The docking was performed in 10 iterations per substrate, with one iteration picked based on binding energy and distance between arginine residues and substrate molecule. The docking image was visualized in PyMOL (PyMOL Molecular Graphics System, Version 2.0 Schrödinger, LLC).

2.9. Statistical analysis

Data are presented as the mean and standard deviation of at least 3 independent experiments.

3. Results

3.1. mUCP3 exchanges malate against phosphate.

First, we investigated whether mUCP3 reconstituted into liposomes transports radioactively labelled ^{14}C-malate against phosphate, using mUCP2 as a positive control [33] and ANT1 as a negative control (Figure 2A). Empty liposomes, in which the exchange should be driven by diffusion over the membrane only were used as an additional negative control (Figure 2A). By comparing the efflux of ^{14}C-malate from proteoliposomes measured over time we concluded that mUCP3 catalyses the malate/phosphate exchange similarly to mUCP2 (Figure 2B). While ANT1 catalyses the exchange of ATP against ADP (Figure S3), it did not induce any significant malate/phosphate exchange, as expected from its tight substrate specificity [52,53]. Thus, we conclude that both, mUCP3 and mUCP2, are active transporter of malate and phosphate. We calculated exchange rates of 9.57 ± 4.39 μM/s (corresponding to 12.0 ± 5.5 mmol/min/$g_{protein}$) and 14.5 ± 3.5 μM/s (18.1 ± 4.4 mmol/min/$g_{protein}$) for mUCP3 and mUCP2, while the rates for empty and ANT1-containing liposomes were 0.19 ± 0.01 μM/s and 0.23 ± 0.09 μM/s, respectively (Figure 2C and Table 1). We also tested whether UCP3-mediated phosphate/malate exchange is inhibited by GTP, GDP and the substrate analogue phenylsuccinate (PS). We measured the amount of ^{32}P-phosphate remaining in the liposomes after 600 s compared to the initial amount at the beginning of the experiment. We found inhibition values of 76.3 ± 18.2 % in the presence of 10 mM GTP, 47.0 ± 2.0 % for 10 mM GDP and 92.2 ± 4.6 % for 20 mM PS (Figures 2D and S4).

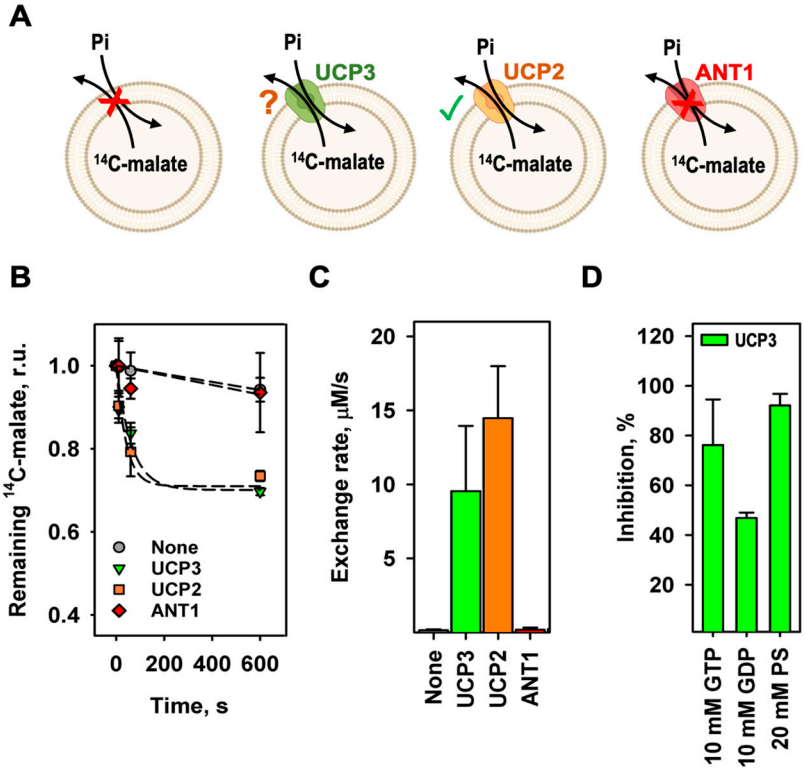

 doi:10.20944/preprints202312.1214.v1

Figure 2. The malate/phosphate exchange is mediated by mUCP3 and mUCP2. (A) Experimental setup to test the mUCP3-mediated malate/phosphate exchange. **(B)** Efflux of malate from liposomes over time measured by remaining intraliposomal ^{14}C-malate radioactivity. Lines are a least-square fit of an exponential function to data. Concentrations of intraliposomal malate and extraliposomal phosphate were 2 mM. Liposomes were measured without protein (grey circles), or with reconstituted mUCP3 (green triangles), or mUCP2 (orange squares), or ANT1 (red diamonds). **(C)** Exchange rate calculated for the malate/phosphate exchange of empty liposomes (first bar), and liposomes containing mUCP3 (second bar), or mUCP2 (third bar), or ANT1 (fourth bar). **(D)** Inhibition of phosphate/malate exchange by GTP, GDP, and phenylsuccinate (PS). Liposomes were filled with 2 mM ^{32}P-phosphate. The extraliposomal substrate was malate at a concentration of 2 mM. Inhibitors were present in both the liposomes and the bulk solution and were added before the start of the exchange. Membranes were made of 45:45:10 mol% PC:PE:CL. Buffer solution contained 50 mM Na_2SO_4, 10 mM Tris, 10 mM MES and 0.6 mM EGTA at pH = 7.34 and T = 296 K. Lipid concentration was 4 mg/ml; protein concentration was 4 μg/(mg of lipid). Data are the mean ± SD of at least three independent experiments.

3.2. The homoexchange of malate and phosphate by mUCP3

Next, we examined the homoexchange of malate and phosphate mediated by mUCP3. We filled mUCP3 containing liposomes either with ^{14}C-malate or ^{32}P-phosphate and measured their release against malate or phosphate, respectively (Inserts in Figure 3A,B). For the comparison, we measured these exchange rates for mUCP2 as well. We found that the malate exchange is higher for mUCP2 (16.6 ± 3.5 μM/s) than for mUCP3 (7.94 ± 1.88 μM/s), while the phosphate exchange is higher for mUCP3 (11.7 ± 3.2 μM/s) compared to mUCP2 (8.00 ± 1.40 μM/s) (Figure 3C and Table 1).

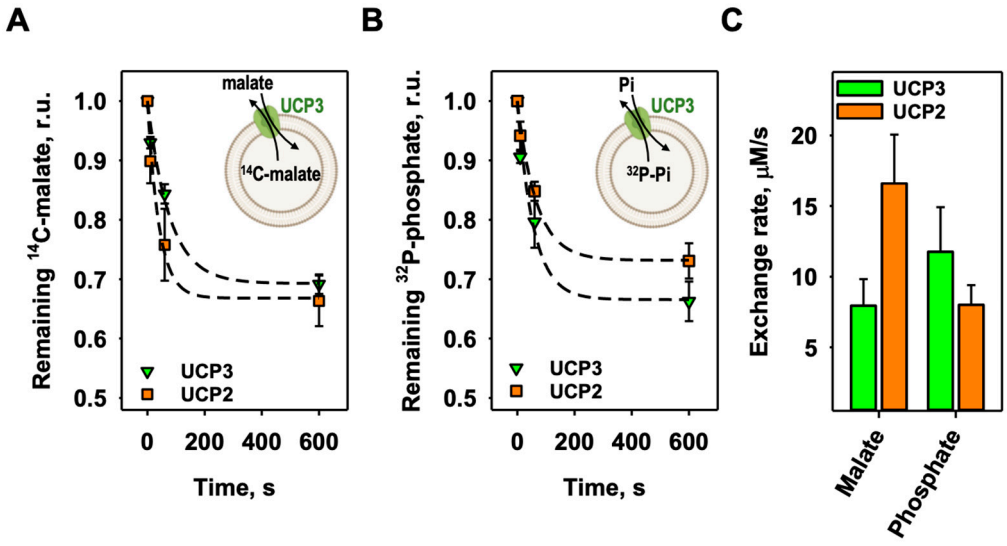

Figure 3. The homoexchange of malate and phosphate is different for mUCP3 and mUCP2. (A) Efflux of malate from liposomes over time measured by remaining intraliposomal ^{14}C-malate radioactivity of mUCP3 (green triangles) or mUCP2 (orange squares). Concentration of intraliposomal and extraliposomal malate was 2 mM. Inset: Experimental setup to test malate/malate homoexchange for mUCP3 (or mUCP2). **(B)** Efflux of phosphate from liposomes over time measured by remaining intraliposomal ^{32}P-phosphate radioactivity of mUCP3 (green triangles) or mUCP2 (orange squares). Concentration of intraliposomal and extraliposomal phosphate was 2 mM. Inset: Experimental setup to test phosphate/phosphate homoexchange for mUCP3 (or mUCP2). Lines in (A) and (B) are a least-square fit of an exponential function to data. **(C)** Exchange rate calculated for the malate/malate exchange (first bar set) and the phosphate/phosphate exchange (second bar set) of mUCP3 (green) and mUCP2 (orange). Membranes were made of 45:45:10 mol% PC:PE:CL. Buffer solution contained 50 mM Na_2SO_4, 10 mM Tris, 10 mM MES and 0.6 mM EGTA at pH = 7.34 and T =

 doi:10.20944/preprints202312.1214.v1

296 K. Lipid concentration was 4 mg/ml; protein concentration was 4 µg/(mg of lipid). Data are the mean ± SD of at least three independent experiments.

3.3. mUCP3 catalyses the heteroexchange of phosphate against various substrates.

In the next step, we analyzed mUCP3-mediated heteroexchange of phosphate against a selection of mitochondrial relevant substrates that were tested for UCP2. We filled UCP3-containing liposomes with ^{32}P-phosphate and measured the release of phosphate (Figures 4A and S5). Since the proteins are randomly inserted into the liposomes (approximately 50:50), we can only globally determine the transport rate but not its directionality. We consider this by assuming that only half of the proteins are involved in the specific exchange. If the exchange of substrates is independent of the protein orientation, the exchange rates determined here would be half the value. We found that the exchange of phosphate against aspartate (19.1 ± 4.6 µM/s), sulfate (14.0 ± 4.1 µM/s) and sulfite (12.9 ± 4.5 µM/s) is higher than against malate (Figure 2). Lower transport rates were observed for oxaloacetate (5.07 ± 1.92 µM/s), thiosulfate (2.70 ± 0.36 µM/s), malonate (1.96 ± 0.72 µM/s), succinate (1.16 ± 0.17 µM/s) and citrate (1.10 ± 0.39 µM/s). In contrast, little to no transport was measured for asparagine (0.40 ± 0.04 µM/s), oxoglutarate (0.37 ± 0.04 µM/s), glutamate (0.29 ± 0.07 µM/s) and glutamine (0.27 ± 0.12 µM/s). All values are also shown in mmol/min/g protein in Table 1. Here, we decided to take twice the "apparent" malate/phosphate exchange rate of empty liposomes (Figure 2) to define non-transported substrates. We tested the same set of substrates on the mUCP2-mediated exchange with phosphate and found strong differences to mUCP3 (Figures 4B and S5). Besides malate, the highest exchange rates were determined for sulfate (18.4 ± 3.7 µM/s) and malonate (16.5 ± 2.0 µM/s). Much lower exchange rates had aspartate (1.31 ± 0.19 µM/s), oxaloacetate (1.26 ± 0.18 µM/s) and citrate (1.14 ± 0.38 µM/s). Very low to no exchange was measured for thiosulfate (0.54 ± 0.36 µM/s), succinate (0.52 ± 0.19 µM/s), glutamate (0.36 ± 0.06 µM/s), oxoglutarate (0.32 ± 0.04 µM/s), asparagine (0.27 ± 0.04 µM/s), sulfite (0.24 ± 0.06 µM/s) and glutamine (0.24 ± 0.02 µM/s) (see also Table 1). While most of the substrates are not transported at all or only at a very slow rate (Figure 4C, white bars), aspartate, oxaloacetate, succinate, sulfite and thiosulfate have a significantly higher exchange rate for mUCP3 compared to mUCP2, with a ratio of exchange rate (k_{UCP3}/k_{UCP2}) of 14.6 ± 4.1, 4.0 ± 1.6, 2.23 ± 0.88, 53.8 ± 23.0 and 5.0 ± 3.4, respectively (Figure 4C, green bars). In contrast, malate and malonate are transported faster by mUCP2, with a ratio of the exchange rates (k_{ucp3}/k_{ucp2}) of 0.66 ± 0.31 and 0.12 ± 0.05, respectively (Figure 4C, orange bars). For citrate (0.96 ± 0.47) and sulfate (0.76 ± 0.27), the exchange rate is almost equal for both proteins (Figure 4C, grey bars). In the absence of any external substrate, we did not observe any significant ^{32}P-phosphate efflux, ruling out phosphate uniport for UCP3 and UCP2 ("None" in Figures 4 and S7).

 doi:10.20944/preprints202312.1214.v1

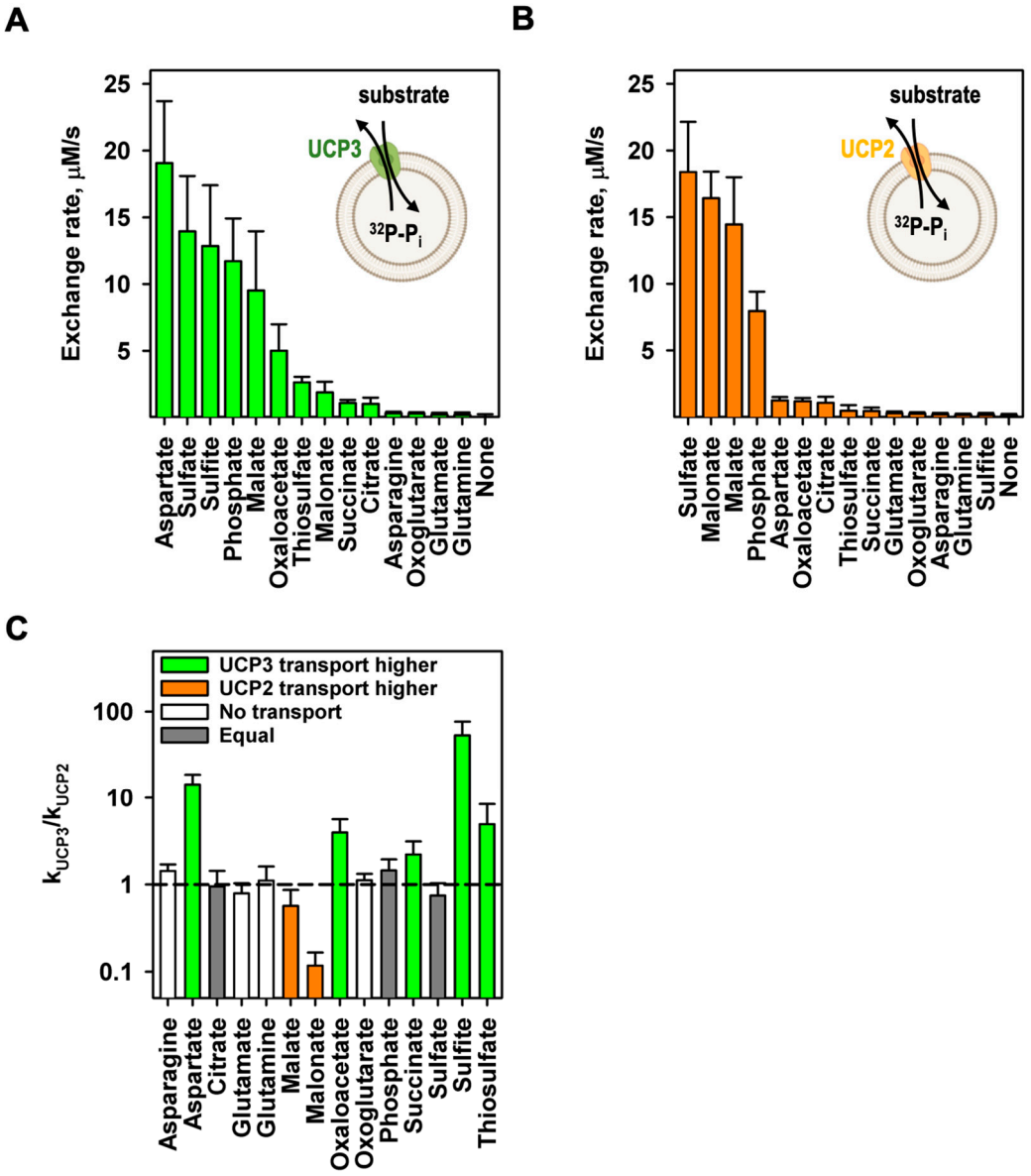

Figure 4. UCP3 catalyzes the heteroexchange of different substrates against phosphate. Exchange rates of mUCP3 **(A)** and mUCP2 **(B)** of the exchange of intraliposomal phosphate against a set of different external substrates sorted by their exchange rate. "None" displays uniport activity of UCP3 and UCP2 measured in the absence of any external substrate. Time course of phosphate efflux for all measurements are shown in Figures S5–S7. **(C)** Ratio of the mUCP3-mediated exchange rates to the mUCP2-mediated exchange rates of the substrates sorted by alphabet. Green bars indicate higher transport rates for the substrates by mUCP3, orange bars for mUCP2. Grey bars indicate similar transport rates for the substrates by mUCP3 and mUCP2. White bars indicate substrates that are not transported by mUCP3 or mUCP2. Experimental conditions are indicated in Figures S5 and S6.

3.4. Arginine 84 (R84) of UCP3 plays a crucial role in mUCP3-mediated substrate exchange.

Finally, we performed static docking experiments to identify most of the existing phosphate binding sites by using the homology model structure of mUCP3 (Figure 1). Since the aspartate/phosphate exchange had highest exchange rate, we also tested the docking of aspartate to mUCP3. We found a high probability for phosphate to bind to R84 and R184 (Figure 5A) and for aspartate to R84 and R278 (Figure 5B). Since R84 appeared in both docking results, we produced the mUCP3R84Q mutant and examined the effect of the mutation on the aspartate/phosphate heteroexchange (Figure 5C). Indeed, the exchange rate was almost 40-fold lower for the R84Q mutant

 doi:10.20944/preprints202312.1214.v1

(0.50 ± 0.08 µM/s, Figure 5D) and comparable with non-transported substrates (Figure 4A, Table 1). Thus, R84 of mUCP3 has a significant impact in the UCP3-mediated heteroexchange of aspartate against phosphate.

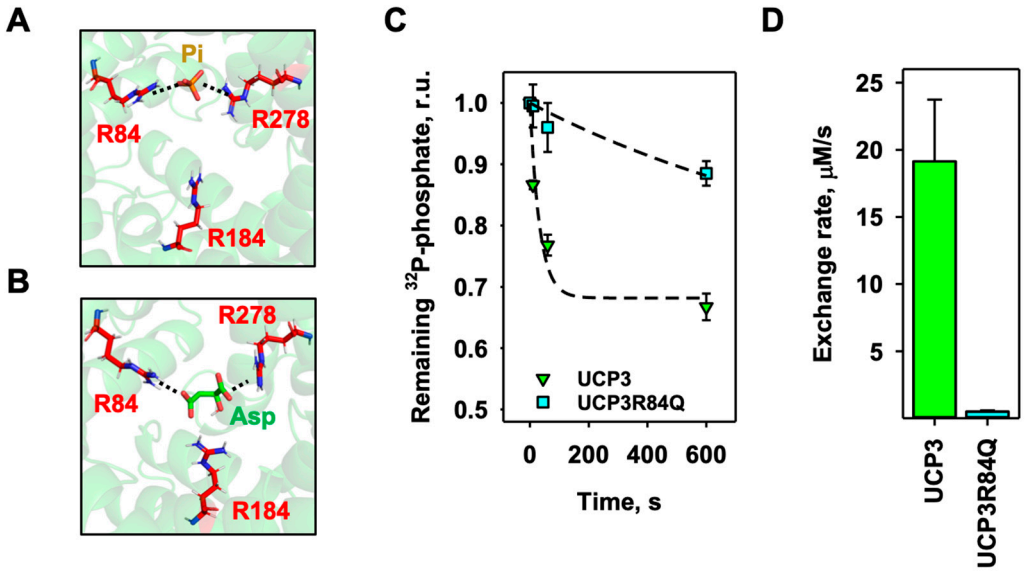

Figure 5. R84 plays an essential role in UCP3-mediated substrate exchange. (A, B) Static docking image of possible interactions of (A) phosphate (P_i) with R84 and R184 and (B) aspartate (Asp) with R84 and R278 in the central binding site of mUCP3. Substrates are displayed as licorice in beige, the amino acids as licorice in cyan, and mUCP3 in cartoon representation in red. (C) Time course of aspartate/phosphate exchange over time of mUCP3 (green) and mUCP3R84Q mutant (cyan) measured by remaining ^{32}P-phosphate radioactivity inside proteoliposomes. Concentration of intraliposomal phosphate and extraliposomal aspartate was 2 mM. (D) Exchange rate calculated for the aspartate/phosphate exchange of mUCP3 (left) and mUCP3R84Q (right). In the experiments, lipid concentration was 4 mg/ml and protein concentration was 4 µg/(mg of lipid). Membranes were made of PC:PE:CL (45:45:10 mol%) and liposomes filled with 2 mM ^{32}P-phosphate. Buffer solution contained 50 mM Na_2SO_4, 10 mM Tris, 10 mM MES and 0.6 mM EGTA at pH = 7.34 and T = 296 K. Data are the mean ± SD of at least three independent experiments.

4. Discussion

Our present results show that mouse UCP3 facilitates membrane transport of negatively charged metabolites which otherwise have a rather low intrinsic membrane permeability [54]. The exchange rate decreases in the order: aspartate > sulfate ≈ sulfite ≈ phosphate ≈ malate >> oxaloacetate >> thiosulfate ≈ malonate ≈ succinate ≈ citrate. These results are similar to those obtained for recombinant human UCP3 in parallel with our study[55]. As mUCP2 and mUCP3 are highly homologous at the substrate binding site (Figure 1), we expected similarities in their substrate specificity. However, there are clear differences between the two proteins: mUCP3 showed its highest exchange rates for aspartate, sulfate and sulfite, whereas mUCP2 transported sulfate and malonate at the highest rate. Because the tissue expression of mUCP2 and mUCP3 is different [28], we suggest that the difference in substrate affinity may be explained by differences in the main tissue metabolism. For example, the export of aspartate catalyzed by UCP3 from mitochondria may play a role in attenuating the development of hypertrophy in cardiomyocytes under stress conditions when cellular metabolism shifts toward glycolysis [56]. By transporting sulfate, UCP3 could contribute to cardioprotection [57]. The highly membrane permeable signaling molecule H_2S [58] is degraded to the membrane impermeable sulfite in the mitochondrial matrix, and sulfite is in turn degraded to sulfate by sulfite oxidase, which is in the intermembrane space. As UCP3 also exhibits a high transport rate for sulfate, it may help to reduce ROS damage in the heart and skeletal muscle by exporting sulfate from the

 doi:10.20944/preprints202312.1214.v1

mitochondria, encouraging further sulfite/sulfate exchange. Human UCP5 and UCP6, which are less homologous to UCP3 than UCP2, have previously been proposed to contribute to ROS regulation by exporting H_2S degradation products, sulfite and thiosulfate, from mitochondria in exchange for sulfate [57]. Thus, it remains an open question whether UCP3 transports sulfoxides. Interestingly, hUCP5 and hUCP6 are also proposed to transport dicarboxylates and aspartate, although to a lesser extent. In addition, the insect UCP4 from *Drosophila melanogaster* was reported to catalyze the homoexchange of aspartate and, with much lower activity, the uniport transport of aspartate [38]. However, uniport transport was not observed for mammalian UCP2, UCP5 and UCP6 [33,59]. Thus, UCP3-mediated uniport transport of aspartate is not supported by the much closer mammalian homologs.

Both mUCP3 and mUCP2 catalyze the homoexchange of phosphate and malate, but with different kinetics. While the homoexchange of mUCP3 is faster for phosphate (compared to mUCP2), the homoexchange of malate is faster for mUCP2 (compared to mUCP3). Substrate homoexchange seems strange at first, but several mitochondrial carriers have been shown to mediate homoexchange, such as the ADP/ATP carrier (ADP and ATP transport in both directions) and the phosphate carrier. Both transport modes are correlated with the metabolic needs of the mitochondria and whether the ATP synthase produces ATP from ADP and phosphate or breaks up ATP into ADP and Pi. The exchange rates determined in this study are of the same order of magnitude for the different mitochondrial carriers and their respective substrates (Table S1). The Pi/Pi homoexchange rate (in mmol/min/g protein) is slightly higher for the phosphate carrier [60] than for UCP3 (PiC: 70 –90; UCP3: 11.7 ± 3.2). In contrast, the malate/malate homoexchange mediated by the citrate carrier (CiC) is lower [61] compared to UCP3 (CiC: 1.98 ± 0.16; UCP3: 7.94 ± 1.88).

The calculated transport rates of mUCP2 in this study are comparable to those reported for other uncoupling proteins [33,38,39]. We generally found a similar substrate specificity for mUCP2, except for citrate, which was reported to be not transported by hUCP2 [33]. The transport rates of malate, malonate, and sulfate where 3- to 6-fold higher in our study, which could be due to the higher concentration of substrates used (2 mM compared to 1 mM [33]. In contrast, the transport rates of aspartate and oxaloacetate are lower [33]. However, it should be emphasized that exchange rates in different studies can be better compared by the determination of the apparent binding constant K_m and the maximum exchange rate V_{max} according to the Michaelis-Menten relation. With the apparent K_m of 1 mM for phosphate [24] and 2.4 ± 0.1 mM for malate [38], the transport rates determined in this paper are expected to be higher than those determined by Vozza et al. Another possible explanation for some of the differences in the results could be that Vozza et al. investigated human UCP2 by measuring ^{32}Pi influx, whereas in the present study mouse UCP2 was investigated by measuring of ^{32}Pi efflux.

Meanwhile, other orthologous uncoupling proteins have been shown to be substrate carriers. Plant UCP1 and UCP2 were functionally characterised as amino acid/dicarboxylate transporters [39], while UCP4A from *Drosophila melanogaster* catalyses the unidirectional transport of aspartate [38]. UCP4 from *Caenorhabditis elegans* was reported to transport succinate, which controls complex II-mediated oxidative phosphorylation [62]. In contrast, several mitochondrial substrate transporters from the SLC25 group such as ATP/ADP carrier (ANT), phosphate carrier (PiC), dicarboxylate carrier (DIC), oxoglutarate carrier (OGC) have been shown to have a protonophoric activity, as a part of a dual transport function.

The importance of the central arginine ring for the binding of the ATP, ADP and fatty acid anion has already been demonstrated for ANT, UCP1 and UCP3 [24,41,44,63,64]. We have hypothesised that the substrate binds in the same region of mUCP3. Indeed, the mutation of R84 resulted in impaired aspartate/phosphate exchange, demonstrating its critical role in substrate transport, and suggesting a mechanism similar to that of ANT1 [44]. The latter involves at least one of the arginines (R79) in the central binding site in the substrate and FA anion transport pathways.

Our results shed light on the possible dual transport function that UCP3 may play in the mitochondrial metabolism of the tissues in which it is expressed. They also highlight the importance

of further investigation of the possible substrate transport function of members of the uncoupling protein family.

Supplementary Materials: The following supporting information can be downloaded at the website of this paper posted on Preprints.org. Figures S1–S7 and Table S1.

Author Contributions: Conceptualization, E.E.P.; funding acquisition, E.E.P.; investigation, T.T, J.K.; project administration, E.E.P.; resources, E.E.P.; supervision, E.E.P., J.K.; writing—original draft, T.T., J.K. and E.E.P.; All authors have read and agreed to the published version of the manuscript.

Funding: This project was supported by the FWF Sonderforschungsbereich F83 and the European Union's Horizon 2020 research and innovation program under the Marie Skłodowska-Curie grant agreement No. 860592 (to E.E.P).

Data Availability Statement: The datasets generated and/or analyzed during the current study can be obtained upon reasonable request from the corresponding authors.

Acknowledgments: We thank Sarah Bardakji for her excellent technical assistance and all members of the Pohl lab for the helpful discussions.

Conflicts of Interest: The authors declare no conflict of interest.

References

1. Palmieri, F. The mitochondrial transporter family SLC25: identification, properties and physiopathology. *Mol Aspects Med* **34**, 465-484 (2013). https://doi.org:10.1016/j.mam.2012.05.005
2. Kunji, E. R. S., King, M. S., Ruprecht, J. J. & Thangaratnarajah, C. The SLC25 Carrier Family: Important Transport Proteins in Mitochondrial Physiology and Pathology. *Physiology (Bethesda)* **35**, 302-327 (2020). https://doi.org:10.1152/physiol.00009.2020
3. Ardalan, A., Smith, M. D. & Jelokhani-Niaraki, M. Uncoupling Proteins and Regulated Proton Leak in Mitochondria. *Int J Mol Sci* **23** (2022). https://doi.org:10.3390/ijms23031528
4. Nicholls, D. G. Mitochondrial proton leaks and uncoupling proteins. *Biochim Biophys Acta Bioenerg* **1862**, 148428 (2021). https://doi.org:10.1016/j.bbabio.2021.148428
5. Palmieri, F., Scarcia, P. & Monne, M. Diseases Caused by Mutations in Mitochondrial Carrier Genes SLC25: A Review. *Biomolecules* **10** (2020). https://doi.org:10.3390/biom10040655
6. Rochette, L. *et al.* Mitochondrial SLC25 Carriers: Novel Targets for Cancer Therapy. *Molecules* **25** (2020). https://doi.org:10.3390/molecules25102417
7. Nedergaard, J. *et al.* UCP1: the only protein able to mediate adaptive non-shivering thermogenesis and metabolic inefficiency. *Biochim Biophys Acta* **1504**, 82-106 (2001). https://doi.org:10.1016/s0005-2728(00)00247-4
8. Nicholls, D. G. A history of UCP1. *Biochem Soc Trans* **29**, 751-755 (2001). https://doi.org:10.1042/bst0290751
9. Ricquier, D. UCP1, the mitochondrial uncoupling protein of brown adipocyte: A personal contribution and a historical perspective. *Biochimie* **134**, 3-8 (2017). https://doi.org:10.1016/j.biochi.2016.10.018
10. Gaudry, M. J. & Jastroch, M. Comparative functional analyses of UCP1 to unravel evolution, ecophysiology and mechanisms of mammalian thermogenesis. *Comp Biochem Physiol B Biochem Mol Biol* **255**, 110613 (2021). https://doi.org:10.1016/j.cbpb.2021.110613
11. Fromme, T. *et al.* Degradation of brown adipocyte purine nucleotides regulates uncoupling protein 1 activity. *Mol Metab* **8**, 77-85 (2018). https://doi.org:10.1016/j.molmet.2017.12.010
12. Beck, V. *et al.* A new automated technique for the reconstitution of hydrophobic proteins into planar bilayer membranes. Studies of human recombinant uncoupling protein 1. *Biochim Biophys Acta* **1757**, 474-479 (2006). https://doi.org:10.1016/j.bbabio.2006.03.006
13. Winkler, E. & Klingenberg, M. Effect of fatty acids on H+ transport activity of the reconstituted uncoupling protein. *J Biol Chem* **269**, 2508-2515 (1994).
14. Klingenberg, M. UCP1 - A sophisticated energy valve. *Biochimie* **134**, 19-27 (2017). https://doi.org:10.1016/j.biochi.2016.10.012
15. Fedorenko, A., Lishko, P. V. & Kirichok, Y. Mechanism of fatty-acid-dependent UCP1 uncoupling in brown fat mitochondria. *Cell* **151**, 400-413 (2012). https://doi.org:10.1016/j.cell.2012.09.010
16. Jezek, P., Orosz, D. E. & Garlid, K. D. Reconstitution of the uncoupling protein of brown adipose tissue mitochondria. Demonstration of GDP-sensitive halide anion uniport. *J Biol Chem* **265**, 19296-19302 (1990).

17. Fleury, C. *et al.* Uncoupling protein-2: a novel gene linked to obesity and hyperinsulinemia. *Nat Genet* **15**, 269-272 (1997). https://doi.org:10.1038/ng0397-269
18. Boss, O. *et al.* Uncoupling protein-3: a new member of the mitochondrial carrier family with tissue-specific expression. *FEBS Lett* **408**, 39-42 (1997). https://doi.org:10.1016/s0014-5793(97)00384-0
19. Krauss, S., Zhang, C. Y. & Lowell, B. B. The mitochondrial uncoupling-protein homologues. *Nat Rev Mol Cell Biol* **6**, 248-261 (2005). https://doi.org:10.1038/nrm1592
20. Garcia-Martinez, C. *et al.* Overexpression of UCP3 in cultured human muscle lowers mitochondrial membrane potential, raises ATP/ADP ratio, and favors fatty acid vs. glucose oxidation. *FASEB J* **15**, 2033-2035 (2001). https://doi.org:10.1096/fj.00-0828fje
21. Zackova, M., Skobisova, E., Urbankova, E. & Jezek, P. Activating omega-6 polyunsaturated fatty acids and inhibitory purine nucleotides are high affinity ligands for novel mitochondrial uncoupling proteins UCP2 and UCP3. *J Biol Chem* **278**, 20761-20769 (2003). https://doi.org:10.1074/jbc.M212850200
22. Jaburek, M. *et al.* Transport function and regulation of mitochondrial uncoupling proteins 2 and 3. *J Biol Chem* **274**, 26003-26007 (1999). https://doi.org:10.1074/jbc.274.37.26003
23. Beck, V. *et al.* Polyunsaturated fatty acids activate human uncoupling proteins 1 and 2 in planar lipid bilayers. *FASEB J* **21**, 1137-1144 (2007). https://doi.org:10.1096/fj.06-7489com
24. Macher, G. *et al.* Inhibition of mitochondrial UCP1 and UCP3 by purine nucleotides and phosphate. *Biochim Biophys Acta Biomembr* **1860**, 664-672 (2018). https://doi.org:10.1016/j.bbamem.2017.12.001
25. Nedergaard, J. & Cannon, B. The 'novel' 'uncoupling' proteins UCP2 and UCP3: what do they really do? Pros and cons for suggested functions. *Exp Physiol* **88**, 65-84 (2003).
26. Mailloux, R. J. & Harper, M. E. Uncoupling proteins and the control of mitochondrial reactive oxygen species production. *Free Radic Biol Med* **51**, 1106-1115 (2011). https://doi.org:10.1016/j.freeradbiomed.2011.06.022
27. Toime, L. J. & Brand, M. D. Uncoupling protein-3 lowers reactive oxygen species production in isolated mitochondria. *Free Radic Biol Med* **49**, 606-611 (2010). https://doi.org:10.1016/j.freeradbiomed.2010.05.010
28. Pohl, E. E., Rupprecht, A., Macher, G. & Hilse, K. E. Important Trends in UCP3 Investigation. *Front Physiol* **10**, 470 (2019). https://doi.org:10.3389/fphys.2019.00470
29. Hilse, K. E. *et al.* The Expression of Uncoupling Protein 3 Coincides With the Fatty Acid Oxidation Type of Metabolism in Adult Murine Heart. *Front Physiol* **9**, 747 (2018). https://doi.org:10.3389/fphys.2018.00747
30. Arsenijevic, D. *et al.* Disruption of the uncoupling protein-2 gene in mice reveals a role in immunity and reactive oxygen species production. *Nat Genet* **26**, 435-439 (2000). https://doi.org:10.1038/82565
31. Xu, X. *et al.* Mitochondrial regulation in pluripotent stem cells. *Cell Metab* **18**, 325-332 (2013). https://doi.org:10.1016/j.cmet.2013.06.005
32. Esteves, P., Pecqueur, C. & Alves-Guerra, M. C. UCP2 induces metabolic reprogramming to inhibit proliferation of cancer cells. *Mol Cell Oncol* **2**, e975024 (2015). https://doi.org:10.4161/23723556.2014.975024
33. Vozza, A. *et al.* UCP2 transports C4 metabolites out of mitochondria, regulating glucose and glutamine oxidation. *Proc Natl Acad Sci U S A* **111**, 960-965 (2014). https://doi.org:10.1073/pnas.1317400111
34. Raho, S. *et al.* KRAS-regulated glutamine metabolism requires UCP2-mediated aspartate transport to support pancreatic cancer growth. *Nat Metab* **2**, 1373-1381 (2020). https://doi.org:10.1038/s42255-020-00315-1
35. Vidal-Puig, A., Solanes, G., Grujic, D., Flier, J. S. & Lowell, B. B. UCP3: an uncoupling protein homologue expressed preferentially and abundantly in skeletal muscle and brown adipose tissue. *Biochem Biophys Res Commun* **235**, 79-82 (1997). https://doi.org:10.1006/bbrc.1997.6740
36. Oliveira, B. A. *et al.* UCP1 and UCP3 Expression Is Associated with Lipid and Carbohydrate Oxidation and Body Composition. *PLoS One* **11**, e0150811 (2016). https://doi.org:10.1371/journal.pone.0150811
37. Silvestri, E. *et al.* Absence of UCP3 influences mitochondrial functionality in brown adipose tissue. *Biochimica et Biophysica Acta (BBA) - Bioenergetics* **1857**, e99-e100 (2016). https://doi.org:10.1016/j.bbabio.2016.04.336
38. Lunetti, P. *et al.* Drosophila melanogaster Uncoupling Protein-4A (UCP4A) Catalyzes a Unidirectional Transport of Aspartate. *Int J Mol Sci* **23** (2022). https://doi.org:10.3390/ijms23031020
39. Monne, M. *et al.* Uncoupling proteins 1 and 2 (UCP1 and UCP2) from Arabidopsis thaliana are mitochondrial transporters of aspartate, glutamate, and dicarboxylates. *J Biol Chem* **293**, 4213-4227 (2018). https://doi.org:10.1074/jbc.RA117.000771

40. Kunji, E. R. & Robinson, A. J. The conserved substrate binding site of mitochondrial carriers. *Biochim Biophys Acta* **1757**, 1237-1248 (2006). https://doi.org:10.1016/j.bbabio.2006.03.021
41. Kreiter, J. *et al.* ANT1 Activation and Inhibition Patterns Support the Fatty Acid Cycling Mechanism for Proton Transport. *Int J Mol Sci* **22** (2021). https://doi.org:10.3390/ijms22052490
42. Andreyev, A. *et al.* The ATP/ADP-antiporter is involved in the uncoupling effect of fatty acids on mitochondria. *Eur J Biochem* **182**, 585-592 (1989). https://doi.org:10.1111/j.1432-1033.1989.tb14867.x
43. Bertholet, A. M. *et al.* H(+) transport is an integral function of the mitochondrial ADP/ATP carrier. *Nature* **571**, 515-520 (2019). https://doi.org:10.1038/s41586-019-1400-3
44. Kreiter, J. *et al.* FA Sliding as the Mechanism for the ANT1-Mediated Fatty Acid Anion Transport in Lipid Bilayers. *International Journal of Molecular Sciences* **24**, 13701 (2023). https://doi.org:ARTN 13701 10.3390/ijms241813701
45. Waterhouse, A. *et al.* SWISS-MODEL: homology modelling of protein structures and complexes. *Nucleic Acids Res* **46**, W296-W303 (2018). https://doi.org:10.1093/nar/gky427
46. Pebay-Peyroula, E. *et al.* Structure of mitochondrial ADP/ATP carrier in complex with carboxyatractyloside. *Nature* **426**, 39-44 (2003). https://doi.org:10.1038/nature02056
47. Rupprecht, A. *et al.* Role of the transmembrane potential in the membrane proton leak. *Biophys J* **98**, 1503-1511 (2010). https://doi.org:10.1016/j.bpj.2009.12.4301
48. Kreiter, J., Beitz, E. & Pohl, E. E. A Fluorescence-Based Method to Measure ADP/ATP Exchange of Recombinant Adenine Nucleotide Translocase in Liposomes. *Biomolecules* **10** (2020). https://doi.org:10.3390/biom10050685
49. Pettersen, E. F. *et al.* UCSF Chimera--a visualization system for exploratory research and analysis. *J Comput Chem* **25**, 1605-1612 (2004). https://doi.org:10.1002/jcc.20084
50. Eberhardt, J., Santos-Martins, D., Tillack, A. F. & Forli, S. AutoDock Vina 1.2.0: New Docking Methods, Expanded Force Field, and Python Bindings. *J Chem Inf Model* **61**, 3891-3898 (2021). https://doi.org:10.1021/acs.jcim.1c00203
51. Trott, O. & Olson, A. J. AutoDock Vina: improving the speed and accuracy of docking with a new scoring function, efficient optimization, and multithreading. *J Comput Chem* **31**, 455-461 (2010). https://doi.org:10.1002/jcc.21334
52. Mifsud, J. *et al.* The substrate specificity of the human ADP/ATP carrier AAC1. *Mol Membr Biol* **30**, 160-168 (2013). https://doi.org:10.3109/09687688.2012.745175
53. Klingenberg, M. The ADP and ATP transport in mitochondria and its carrier. *Biochim Biophys Acta* **1778**, 1978-2021 (2008). https://doi.org:10.1016/j.bbamem.2008.04.011
54. Hannesschlaeger, C., Horner, A. & Pohl, P. Intrinsic Membrane Permeability to Small Molecules. *Chem Rev* **119**, 5922-5953 (2019). https://doi.org:10.1021/acs.chemrev.8b00560
55. De Leonardis, F. *et al.* Human mitochondrial uncoupling protein 3 functions as a metabolite transporter. *FEBS Lett* (2023). https://doi.org:10.1002/1873-3468.14784
56. Ritterhoff, J. *et al.* Metabolic Remodeling Promotes Cardiac Hypertrophy by Directing Glucose to Aspartate Biosynthesis. *Circulation Research* **126**, 182–196 (2020).
57. Gorgoglione, R. *et al.* The human uncoupling proteins 5 and 6 (UCP5/SLC25A14 and UCP6/SLC25A30) transport sulfur oxyanions, phosphate and dicarboxylates. *Biochimica et biophysica acta. Bioenergetics* **1860**, 724—733 (2019).
58. Mathai, J. C. *et al.* No facilitator required for membrane transport of hydrogen sulfide. *Proc Natl Acad Sci U S A* **106**, 16633-16638 (2009). https://doi.org:10.1073/pnas.0902952106
59. Gorgoglione, R. *et al.* The human uncoupling proteins 5 and 6 (UCP5/SLC25A14 and UCP6/SLC25A30) transport sulfur oxyanions, phosphate and dicarboxylates. *Biochim Biophys Acta Bioenerg* **1860**, 724-733 (2019). https://doi.org:10.1016/j.bbabio.2019.07.010
60. Stappen, R. & Kramer, R. Functional properties of the reconstituted phosphate carrier from bovine heart mitochondria: evidence for asymmetric orientation and characterization of three different transport modes. *Biochim Biophys Acta* **1149**, 40-48 (1993). https://doi.org:10.1016/0005-2736(93)90022-r
61. Bisaccia, F., De Palma, A. & Palmieri, F. Purification and reconstitution of the tricarboxylate carrier from rat liver mitochondria. *Ital J Biochem* **39**, 167A-169A (1990).
62. Pfeiffer, M. *et al.* Caenorhabditis elegans UCP4 protein controls complex II-mediated oxidative phosphorylation through succinate transport. *J Biol Chem* **286**, 37712-37720 (2011). https://doi.org:10.1074/jbc.M111.271452

 doi:10.20944/preprints202312.1214.v1

63. Wang, Y. & Tajkhorshid, E. Electrostatic funneling of substrate in mitochondrial inner membrane carriers. *Proc Natl Acad Sci U S A* **105**, 9598-9603 (2008). https://doi.org:10.1073/pnas.0801786105
64. Mavridou, V. *et al.* Substrate binding in the mitochondrial ADP/ATP carrier is a step-wise process guiding the structural changes in the transport cycle. *Nat Commun* **13**, 3585 (2022). https://doi.org:10.1038/s41467-022-31366-5